1989

NASA/ASEE SUMMER FACULTY FELLOWSHIP PROGRAM

MARSHALL SPACE FLIGHT CENTER
The University of Alabama in Huntsville

Radial Response of the Burst And Transient Source Experiment

Prepared by:	John Patrick Lestrade
Academic Rank:	Assistant Professor
University and Department:	Mississippi State University Department of Physics and Astronomy
NASA/MSFC:	
Laboratory:	Space Science
Division:	Astrophysics
Branch:	High-Energy Astrophysics
MSFC Colleague:	G. J. Fishman
Date:	July 21, 1989
Contract No.:	The University of Alabama in Huntsville NGT-01-008-021

Radial Response of the Burst And Transient Source Experiment

by

John Patrick Lestrade
Assistant Professor of Physics and Astronomy
Mississippi State University
Mississippi State, Mississippi, 39762

Abstract

The Gamma Ray Observatory includes four experiments designed to observe the gamma-ray universe. Jerry Fishman in the High Energy Astrophysics Branch at Marshall Space Flight Center is the principal investigator for one of these experiments, the Burst And Transient Source Experiment (BATSE).

During my first summer with the BATSE team in 1988, we completed laboratory measurements to test the response of the BATSE modules to gamma-ray sources that are non-axial. The results of these observations are necessary for the correct interpretation of BATSE data obtained after it is put in Earth orbit.

Subsequent analysis of the data revealed a shift in the centroids of the full-energy photopeaks for angles of incidence between about 70° and 110°. This effect was diagnosed as being due to a radial dependence of the light collecting efficiency of the large-area detector (LAD). Energy-depositing events that occur near the perimeter of the 10-inch radius NaI disc are not as efficiently collected as those events that occur near the disc's center.

In this report we analyze this radial response and in so doing we are able to explain the non-gaussian shape of the photopeaks seen in the spectra taken at all angles.

Acknowledgements:

The summer of 1989 has been another chapter in the exciting story of my association with the High Energy Astrophysics group at the Marshall Space Flight Center. My colleagues have given unselfishly of their time and expertise to make me an integral part of the group. I appreciate all that I have learned from them. I am sincerely grateful for their acceptance and friendship.

In particular I would like to thank Jerry Fishman for the opportunities that he has provided me. His patience with my naïve questions has been of immeasurable help.

I am also indebted to Dr. Edward West of the Solar Physics Branch of MSFC for his help in converting data from eight-inch floppy diskettes to a PC-compatible format. Several times during this past summer I have called upon him and each time he has unhesitatingly provided help.

The administrative aspects of a program this large are quite complex. It is a credit to Frank Six, Jerry Karr, and Mike Freeman that it appears to us, the visiting faculty, to run so effortlessly.

Finally, I would be remiss if I didn't also show appreciation for the support and friendship of Chip, Tom, John, Scott, Jeff, Philip, Bob, Bill, Bob, Billy Bob, and Ellen.

John Patrick Lestrade
July 21, 1989

List of Figures

1. Introduction:

1.1 The Gamma-Ray Observatory

Before the year 2000 NASA plans to launch more than 9 major space missions. These observatories will study the universe in the infrared, visible, ultraviolet, x-ray, and gamma-ray portions of the spectrum. The objects to be studied include the earth, the planets, the sun, and other more exotic, cosmological objects in which high-energy processes are taking place.

One of the more enigmatic objects that will be studied is the gamma ray burster (GRB). Since the discovery of the first in 1969 we have recorded hundreds of these peculiar objects. The frequency of discovery has reached approximately one GRB every two days.

The spectra of GRB's are confined almost totally to the gamma ray portion of the spectrum. The is quite strange for explosive astronomical bodies. Attempts to locate visual counterparts have been only partially successful. This inability to locate a companion means it is also difficult to assign distances to GRB's and therefore their absolute magnitudes remain unknown. Typical burst durations are on the order of tens of seconds with the shortest being measured in milliseconds and the longest several minutes. In general they show very short rise times and somewhat longer decays. Further, several GRB's display periodicities in brightness during the decay phase. Current GRB models adopt a neutron star as the primary source of energy. An excellent review of gamma-ray bursters has been given by Hurley (1989).

All agree that better data are needed. Higher resolution in time, space, and energy are necessary to eliminate the dozens of models which currently abound. Fortunately, this improvement in GRB data is imminent. One major, earth-orbiting platform for the study of GRB's is nearing completion. The Gamma Ray Observatory (GRO) is, at the time of this writing, undergoing final testing before its launch in the summer of 1990.

GRO is a 17-ton satellite carrying 4 experiments; the Oriented Scintillation Spectrometer Experiment (OSSE), the Imaging Compton Telescope (COMPTEL), the Energetic Gamma-Ray Experiment (EGRET), and the Burst And Transient Source Experiment (BATSE). Together, these instruments detect gamma radiation at energies from 30 keV to 30 GeV. GRO is scheduled to be launched to a nominal altitude of 250 miles (450 km). Its nominal lifetime is five years.

The High-Energy Astrophysics Branch in the Space Science Laboratory at Mar-

shall Space Flight Center has designed, built, and is now testing the BATSE detectors. As a NASA/ASEE Summer Faculty Fellow I have been involved in some of the laboratory testing of the BATSE modules and in the analysis of the acquired data.

1.2 Burst And Transient Source Experiment

BATSE is composed of eight detector modules (Figure 1). These modules will be situated at the eight "corners" of GRO. In this orientation it is able to monitor the complete sky except for that part temporarily blocked by the earth. As the name implies, BATSE is designed to observe and record gamma-ray events that are short-lived. Although its raison d'être is the study of gamma-ray bursters, it also has been designed to observe sources of gamma radiation that are long-lived – such as the sun, pulsars, and black holes.

The principal detector in each module is called the Large-Area detector (LAD). This is a sodium iodide crystal in the shape of a disc with a diameter of 20 inches and a thickness of 0.5 inches. The shape and size of the crystal were chosen to make BATSE more sensitive to the low-energy gamma ray spectrum (i.e., 30 keV$\sim$ 240 keV) and to permit the measurement of very weak sources.

1.2.1 BATSE Testing and Calibration

One of the problems inherent in an observational science is the effect that the observer's instrument has on the data. That is, given a uniquely-valued input, the output contains a finite spread in values reflecting the instrument's nature. In the case of a gamma-ray instrument, such as BATSE, there are contributions to this dispersion from inhomogeneities in the crystal, statistical fluctuations in the conversion of gamma-ray energy into an electrical signal, electronic noise, and other sources. Each of these contributions tends to spread the monoenergetic input into an approximate gaussian shape (Price, 1964). Examples of the resultant output spectra are shown in Figure 2. As seen here, a typical gamma-ray spectrum has additional complexity. Not only is the input energy spread into a wide peak (cf. 662 keV peak in Figure 2), but scattering events which result in only partial deposition in the crystal add other features to the spectrum.

When a monoenergetic beam of photons strikes the sodium iodide crystal in the detector, some of the photons are completely converted into an electrical response that becomes recorded as counts in one of the channels of the photopeak. However, some photons deposit only part of their energy and are scattered out of the detector. These become recorded as lower-energy events and show up as counts in the Compton continuum. Still other photons lose some energy outside of (often

behind) the crystal and are then scattered back into the crystal where they become recorded as counts in the backscatter peak. As seen in this figure, even when the input is monoenergetic, these effects distort the spectrum in a very complicated way. When the source is *not* monoenergetic, as in the case of gamma ray bursters, the situation is considerably more complicated.

Figure 3 presents an observation of a gamma-ray burster (Metzger *et. al.*, 1974). The exponentially decaying energy spectrum is typical of these events and is consistent with a model based on thermal bremstrahlung. These are certainly more complicated than the monoenergetic case. Before we can determine the true spectrum that was *incident* on the detector, we must solve a complicated problem that depends on how the detector responds to incident photons. This response is a function of not only the incident energy but also of the angle of incidence. At MSFC part of our responsibility is to provide a response matrix that describes the detector's effects on an input spectrum. To this end we have spent the past year and a half measuring the spectra with several sources under various conditions. This report presents results of the radial response tests.

2. Radial Response: TPS-119

During a gamma-ray event for BATSE in earth orbit there are at least four detectors responding to the flux of radiation. Since these detectors are oriented in different directions, it is important to know how the detector response changes as a function of the angle of incidence.

The expected effect is the decrease in efficiency due to the smaller projected area as the crystal is turned relative to the flux. This decrease was observed. What was also observed, but not fully expected, was a shift in the peak centroids as the crystal was rotated. In other words the observed energy of the incident beam *decreased* as the angle of incidence changed from 70° to 90°. This decrease for Cs-137 and Se-75 photopeaks is shown in Figure 4. The total angular dependence of this decrease is complicated and is discussed in greater detail by Lestrade (1988). In this report we are primarily concerned with the implications of this secondary effect – the apparent decrease of the incident energy with increasing angle of incidence.

The discovery of the shift in the centroids of the full-energy photopeaks for angles of incidence between about 70° and 90° was diagnosed as being due to a radial dependence of the light collecting efficiency of the large-area detector (LAD). Measurements showed that for energy deposited near the perimeter, the detector has a light collection efficiency that is about 12% less than for that deposited near the center. This is not a property of the scintillator, but rather, a property of the light-collection process. As the crystal is turned the principal area of energy deposition moves from the whole disc at 0° to that local area of the perimeter facing the

source at 90°. Therefore, when the crystal is illuminated at any angle, the output is a superposition of many gaussians, not centered about the true centroid, but shaded to the left (i.e., lower energies).

At angles near 0° the resultant photopeak shows contributions from all areas of the disc. However, for angles of incidence near 90° (or 270°) the photopeak is representative of only the perimeter.

The former effect is seen in Figure 5. This figure presents the 662 keV peak of Cs-137 at an angle of 0°. Note that at normal incidence the peak is a superposition of gaussians. The theoretical gaussian shown in this figure has a centroid at 662 keV. Similar spectra taken at 266°, on the other hand, peak at a lower energy, are less dispersed, and show a purer gaussian shape because they arise from a more localized region of the crystal (cf. Lestrade, 1988).

2.1 Disc Integration

If we assume azimuthal symmetry, then the centroids of the individual gaussians that constitute the photopeak are functions of only the radius, r. In this case, the contribution from the annulus between r and $r + dr$ of the LAD is the simple gaussian given by

$$2\pi r dr e^{-\alpha(E-E_0(r))^2}, \tag{1}$$

where α is a constant yet to be determined, and the centroid position $E_0(r)$ is the radial response. The total photopeak, $P(E)$, in counts per channel is therefore given by the integration of these annuli from disc center to perimeter, viz.

$$P(E) = \int_0^{10} 2\pi r e^{-\alpha(E-E_0(r))^2} dr. \tag{2}$$

One might expect, given a measured spectrum $P(E)$, to be able to solve Equation (2) for $E_0(r)$. This is not an easy task. We decided to approach the problem in a more straight-forward way – we would directly measure $E_0(r)$.

2.1 Measurement of the Radial Response

The table below lists the radioactive sources used in this test. The Am-241 and Na-22 sources were used on only detector DM 1. Mercury-203 was used for all nine modules (eight flight and one protoflight). For the purposes of this report and historical reasons the modules are numbered 1-7, 0/8, and 'P'.

Radioactive Sources Used in Radial Response			
Isotope	${}^{A}_{Z}$Symbol	Half-Life	Energies (MeV)*
Americium-241	${}^{241}_{95}$Am	458 yr.	59.5
Mercury-203	${}^{90}_{203}$Hg	47 d.	[72.9], 279.2
Sodium-22	${}^{22}_{11}$Na	2.62 yr.	511, 1275

* underscore indicates coincident gammas, square brackets indicate sum peaks.

With a source holder and collimator especially built for this test, we were able to restrict the gamma-ray flux to local regions of the disc (Figure 6). Fifteen radial positions as shown in Figure 7 were chosen. The illuminated spot size on the disc was calculated to be approximately 0.75 inches. By illuminating such a small region we were hoping to measure 1) the shift in peak centroid as the holder was moved across the face of the crystal and 2) the width of the gaussians that were a result of the electronic response of the instrument and not contaminated by the combination of gaussians from all portions of the disc.

2.2 Results

Figure 8 presents three Hg-203 spectra to show the shift in peak centroid with increasing radial position. There is minimal shift in the centroid for points as far out as 6 inches from the disc center. However, at 9.5 inches the shift is significant.

Figure 9 presents the centroid positions for modules 1 through 3 as a function of radius for Hg-203. (In this and following radial response figures, the data from the left and right sides of the disc are averaged.) Note the singular depression in the radial response for DM 1 near the disc center. At first we thought that this may have been caused by an error in measurement. However, as Figure 10 shows, the same deficiency is evident in the spectra of all nuclides when DM 1 is used. Further checking found the culprit – a small piece of tin purposely left in the center of this module after removal of an unneeded light sensor. Its presence will not affect other measurements. Included in this figure are the formulae for the energy of the centroid as a quadratic in radius for these three peaks.

For completeness Figure 11 and Figure 12 present the centroid positions vs. radius for the 279 keV peak for the remaining 6 modules.

With an idea of the width of the gaussians from the localized regions of the disc and the radial dependence of the centroids of these peaks, we thought it would be interesting to try to reconstruct the photopeaks measured in full-disc illumination by substituting for α and $E_0(r)$ and performing the integration in equation (2). In order to simplify the functional form of the radial response, $E_0(r)$, we assumed a

constant centroid position for gaussians formed within a distance r_0 of disc center and a linear decrease from that point to the perimeter. Three such functions along with the measurements of the 279 keV peak are shown in Figure 13. Remembering that the depression at $r = 0$ is not representative of what is actually going on near the center, this simple model fits the radial response quite well.

The radial response function in this case is given by

$$E_0(r) = \begin{cases} \mathcal{E}_0 & 0 \le r < r_0; \\ \frac{(10-r(1-f)-fr_0)}{(10-r_0)}\mathcal{E}_0 & r_0 \le r \le 10. \end{cases} \quad (3)$$

where $\mathcal{E}_0$ is independent of r and equals the centroid position for gaussians that result from events where $r < r_0$ and f is the "edge deficiency" or fractional shift in centroid position for gaussians originating from the perimeter. For example, in figure 12 $f = 0.12$ and $r_0 = 5$ in.

With this function, equation (2) reduces to

$$P(E) = \int_0^{r_0} 2\pi r e^{-\alpha(E-\mathcal{E}_0)^2} dr + \int_{r_0}^{10} 2\pi r e^{-\alpha\{E-\mathcal{E}_0[10-r(1-f)-fr_0]/(10-r_0)\}^2} dr, \quad (4)$$

Performing the first integration gives

$$\pi r_0^2 e^{-\alpha(E-\mathcal{E}_0)^2} + \int_{r_0}^{10} 2\pi r e^{-\alpha\{E-\mathcal{E}_0[10-r(1-f)-fr_0]/(10-r_0)\}^2} dr. \quad (5)$$

3. Conclusions

The three variables in this model are thus f, r_0, and α. However, these are not totally free variables. They are constrained by the radial response measurements as shown in Figures 8-10. Still, even with these restrictions the results are very good.

Figure 14 presents the Cs-137 662 keV peak (from Figure 5) along with $P(E)$ calculated from Equation 5 for the three cases of edge deficiencies of 10%, 12%, and 14%. The data are clearly much better fit by the 12% case.

The next figure (Figure 15) shows the same peak but with $P(E)$ calculated for an edge deficiency of 12% and center radii, r_0, of 5, 5.5, and 6 in. Here an r_0 of 5.5 in. provides a better fit.

Finally Figure 16 shows that an α near 0.020 is correct.

It is reassuring that these parameters are independent and in rough agreement with the radial response test results. For example, Figures 8 and 11 indicate that an edge deficiency of 12% and an r_0 of 5.5 are reasonable values.

Pendleton (1989) recently used the quadratic fits to radial response in his Monte Carlo simulation of a mercury-203 spectrum in the Absolute Efficiency Tests (TPS-118). Figure 17 shows a comparison of the observations with his calculated spectrum.

There are still several questions that remain unanswered about the effect of the LAD radial response on the output photopeaks. For example, several Na-22 511 keV photopeaks measured during the science tests in 1988 (TPS-59) showed a double-peak structure. At that time we attributed this to cracks in the crystal structure. It would be interesting to see if a "simple" radial response function could explain at least part of this shape.

Bibliography

1. Hurley, K., 1989, Cosmic Gamma-Ray Bursts, Lectures given at the NATO Adv. Studies Inst., Erice, Italy, April, 1988.

2. Lestrade, J. P. (1988) Angular Response Calibration of the Burst And Transient Source Experiment. *NASA Technical Reports*, **CR-183553**, XIX:1-35.

3. Metzger, A. E., R. H. Parker, D. Gilman, L. E. Peterson, and J. I. Trombka, 1974, Observation of a Cosmic Gamma-Ray Burst on *Apollo 16*. I. Temporal Variability and Energy Spectrum, *Astrop. J.*, **194**, L19-L25.

4. Pendleton, G. E., 1989, Private communication.

5. Price, W. J., 1964, Nuclear Radiation Detection, Second Edition, McGraw-Hill Book Company, New York.

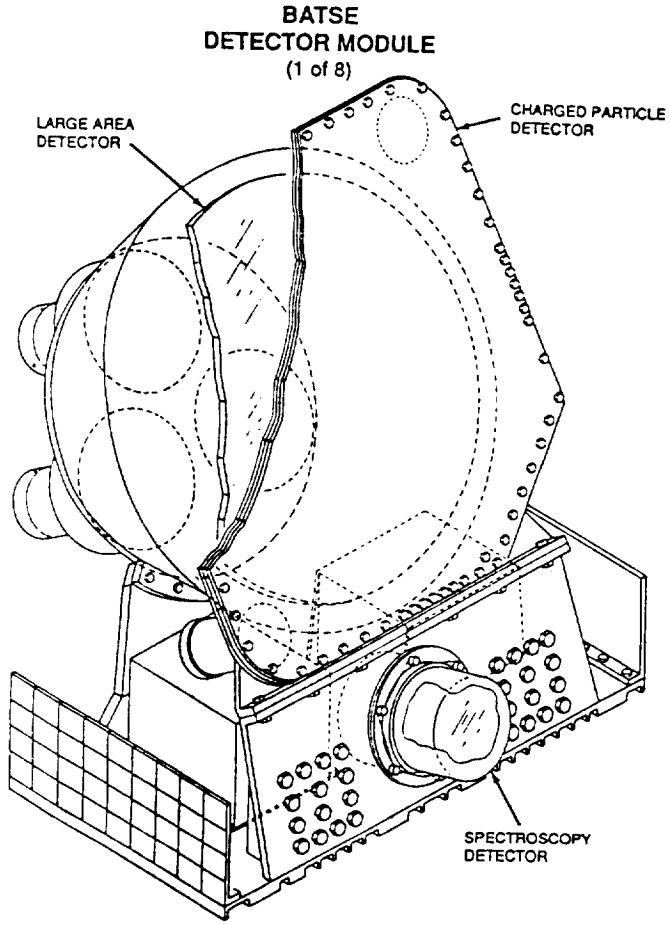
BATSE
DETECTOR MODULE
(1 of 8)
LARGE AREA
DETECTOR
CHARGED PARTICLE
DETECTOR
SPECTROSCOPY
DETECTOR

Figure 1

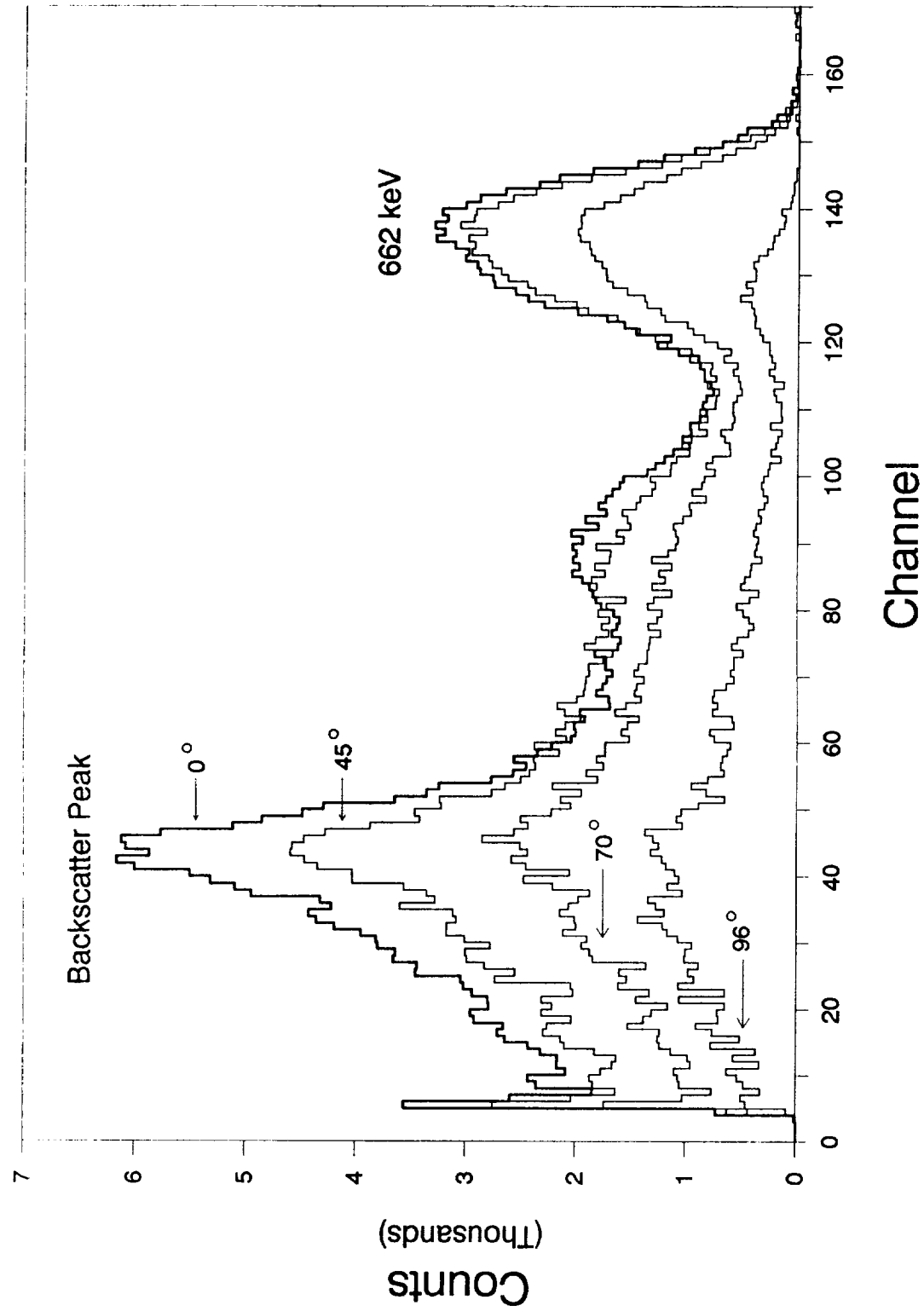
Backscatter Peak
662 keV
0°
45°
70°
96°
Counts
(Thousands)
Channel
0
1
2
3
4
5
6
7
0
20
40
60
80
100
120
140
160

Figure 2

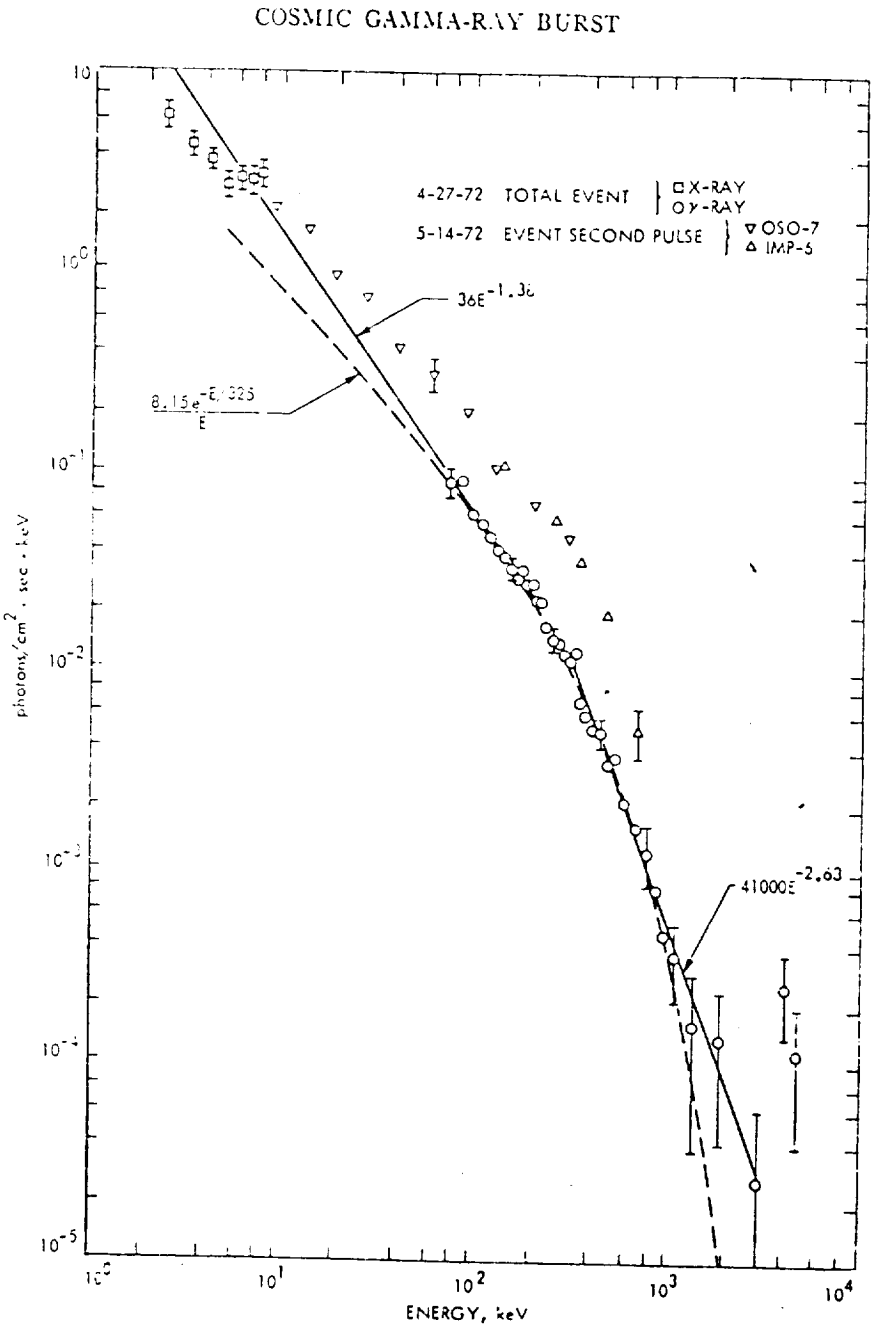

Figure 3

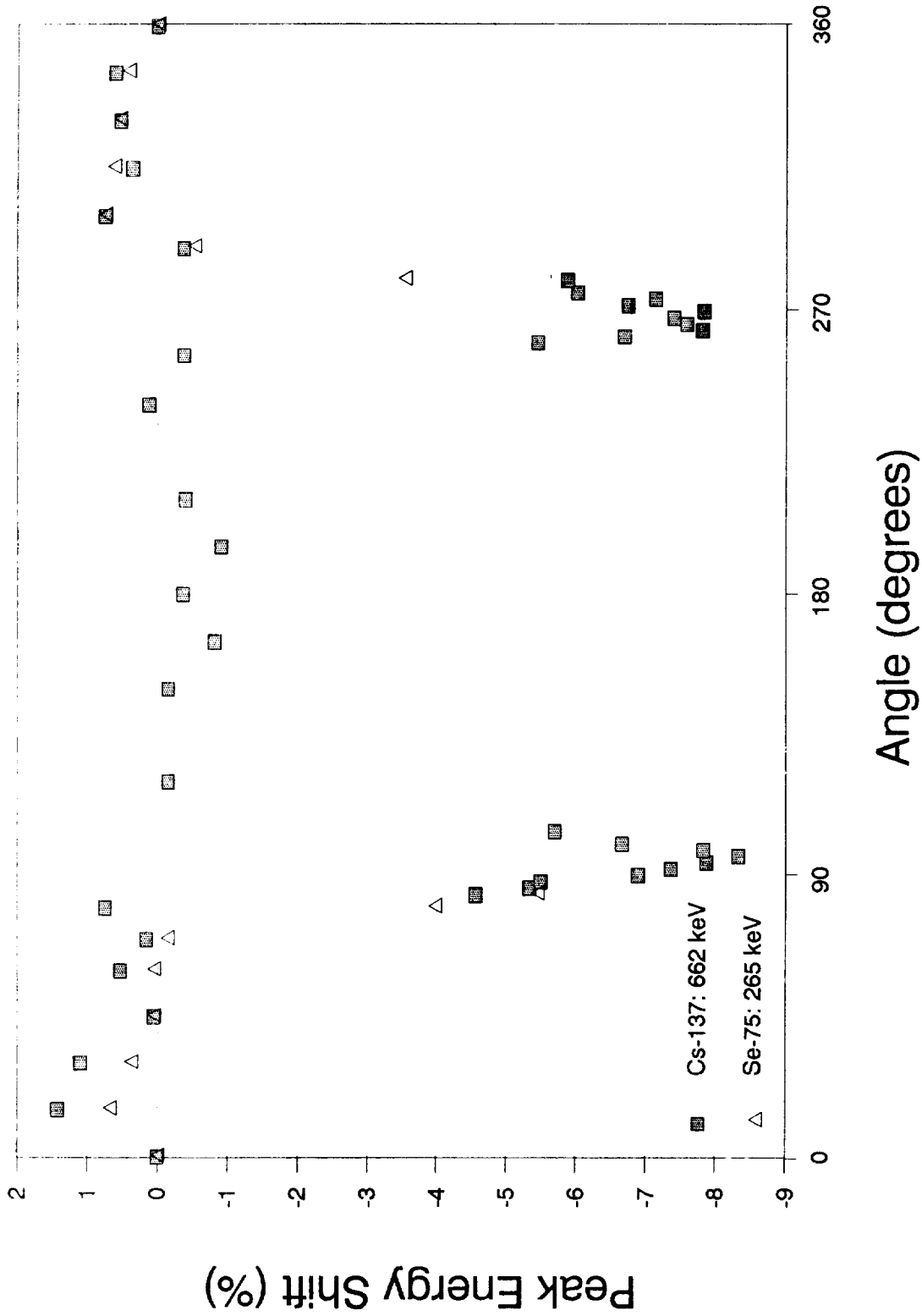

Figure 4

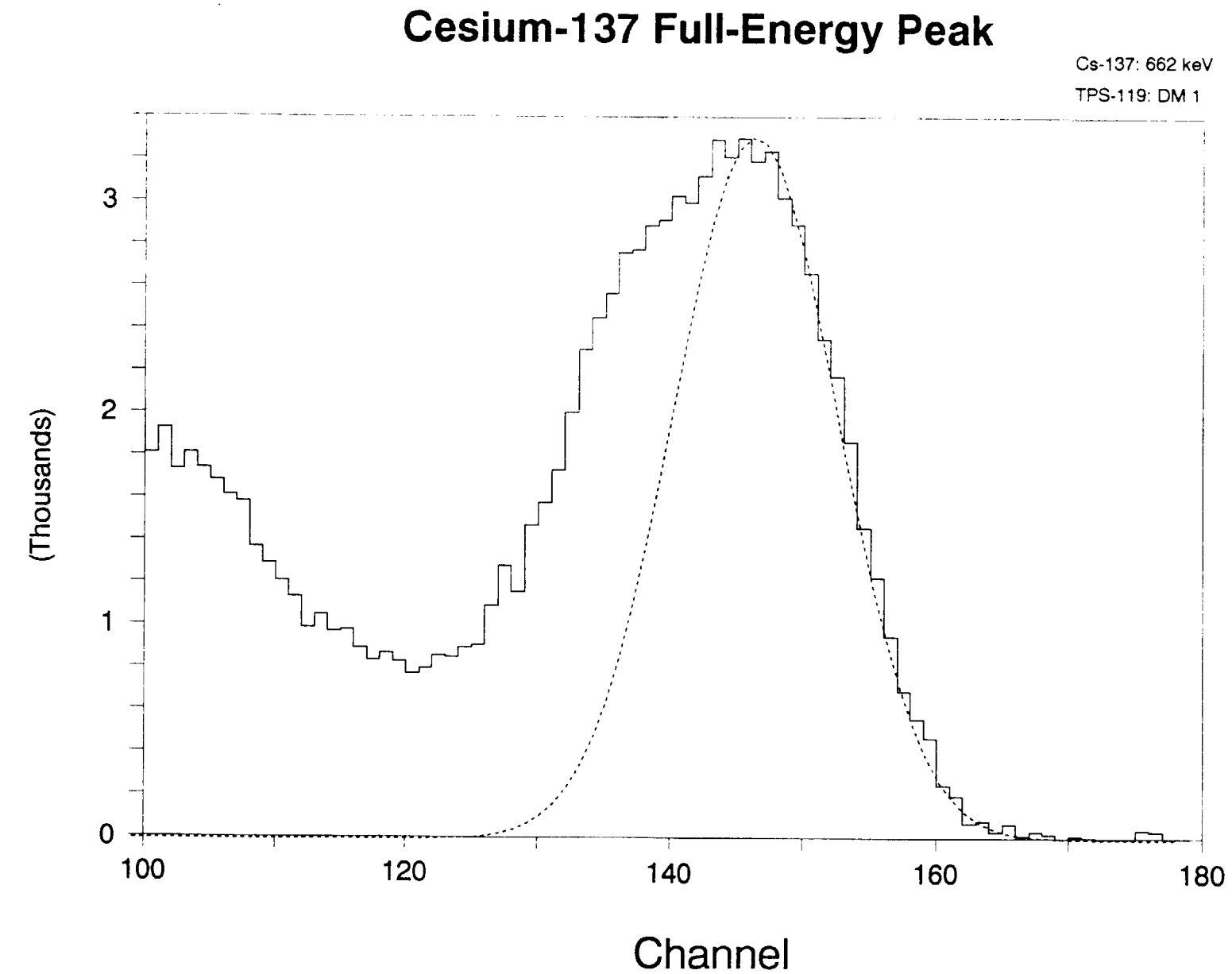
Cesium-137 Full-Energy Peak
Cs-137: 662 keV
TPS-119: DM 1
Counts
(Thousands)
3
2
1
0
100
120
140
160
180
Channel

Figure 5

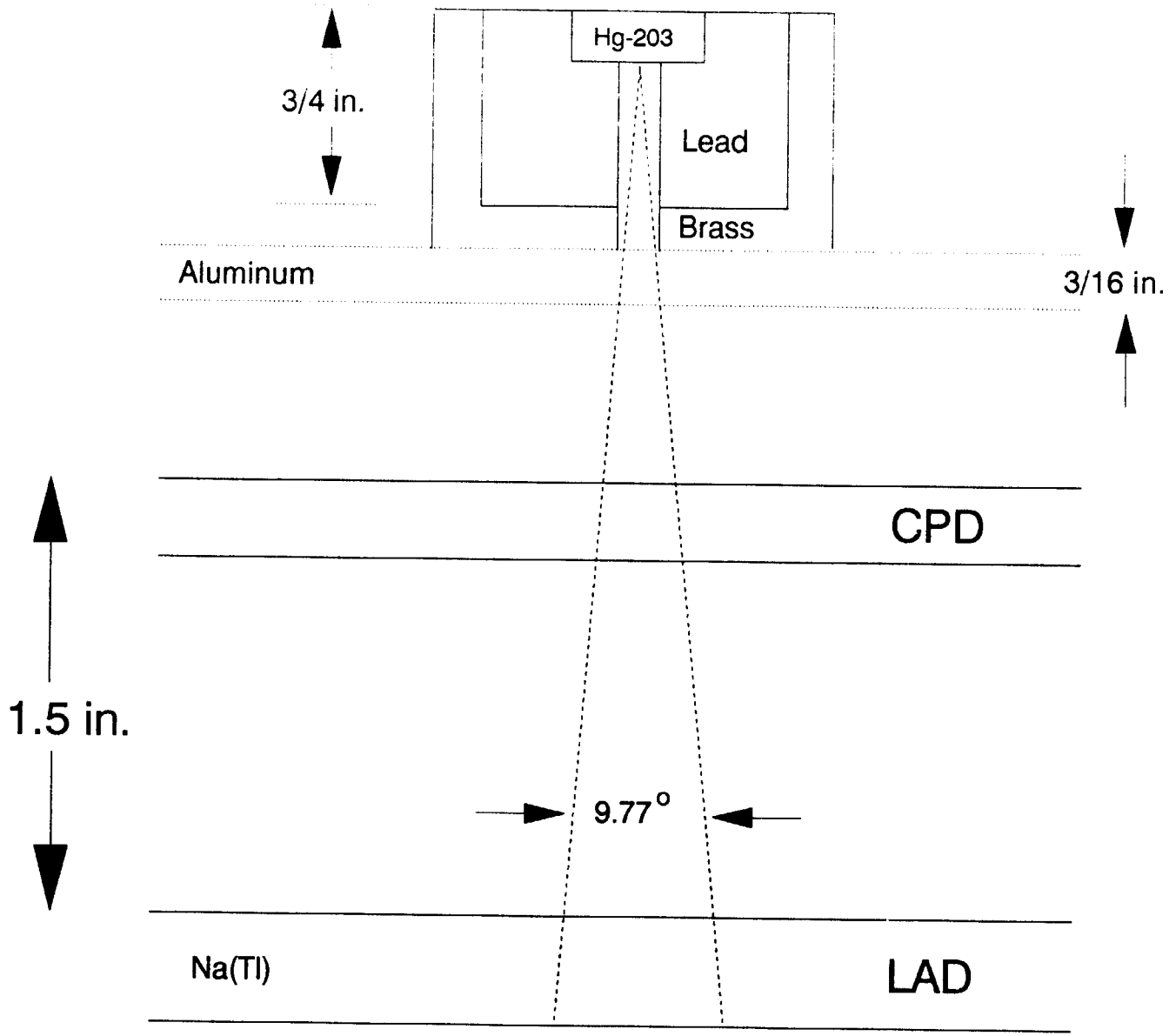

Source Holder: TPS-119

Figure 6
XVIII-14

Radial Positions for TPS-119

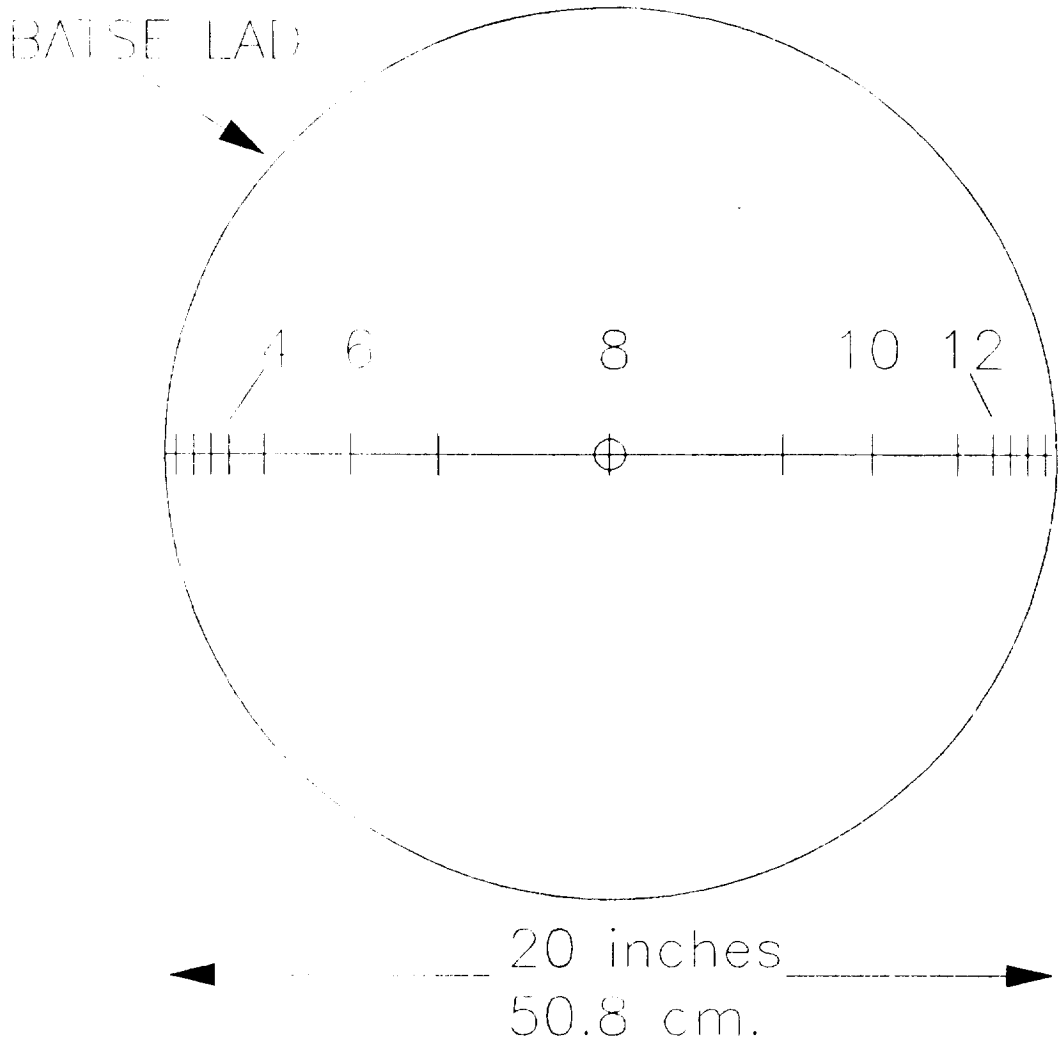

Figure 7

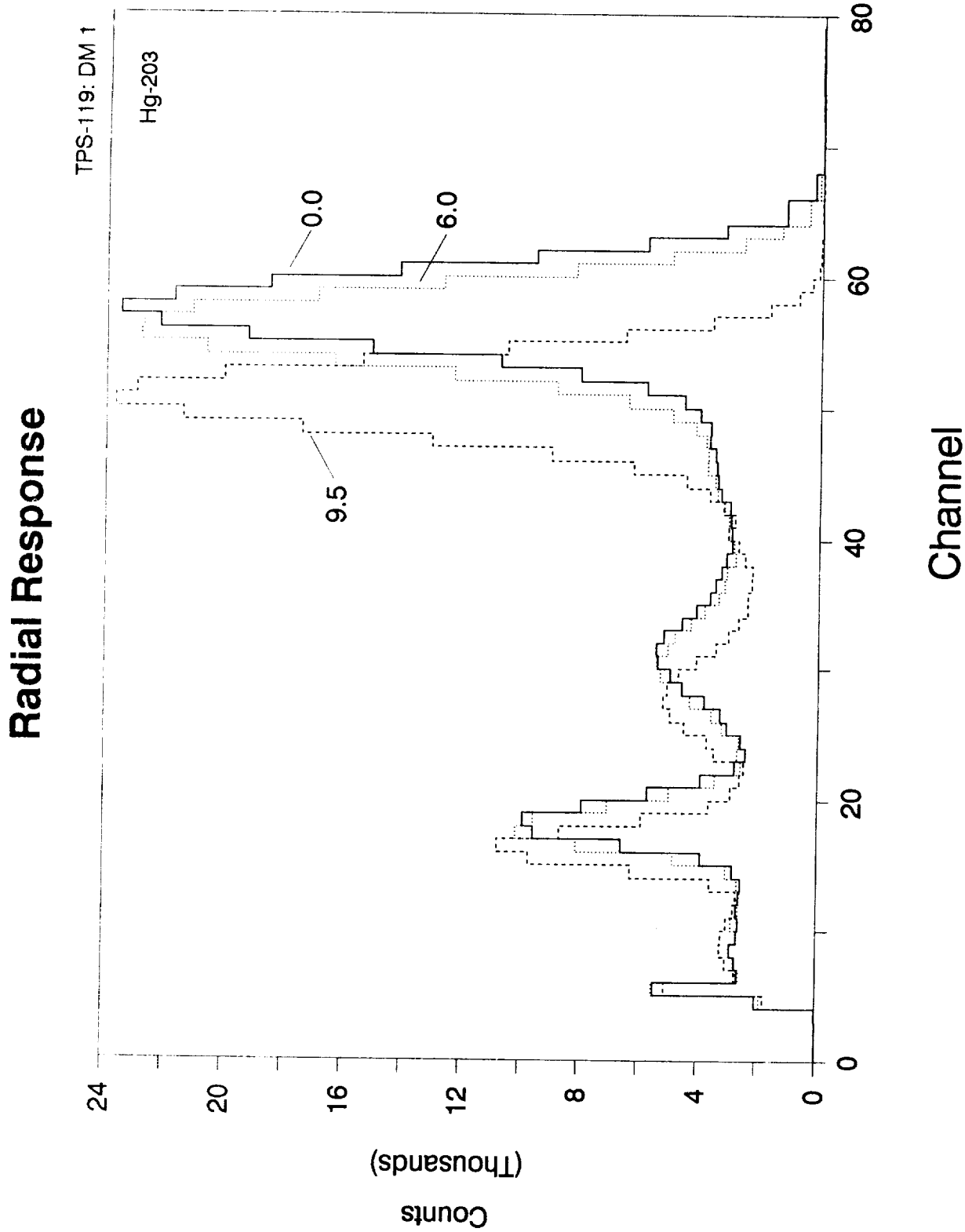
Radial Response
TPS-119: DM 1
Hg-203
0.0
6.0
9.5
Counts
(Thousands)
0
4
8
12
16
20
24
0
20
40
60
80
Channel

Figure 8

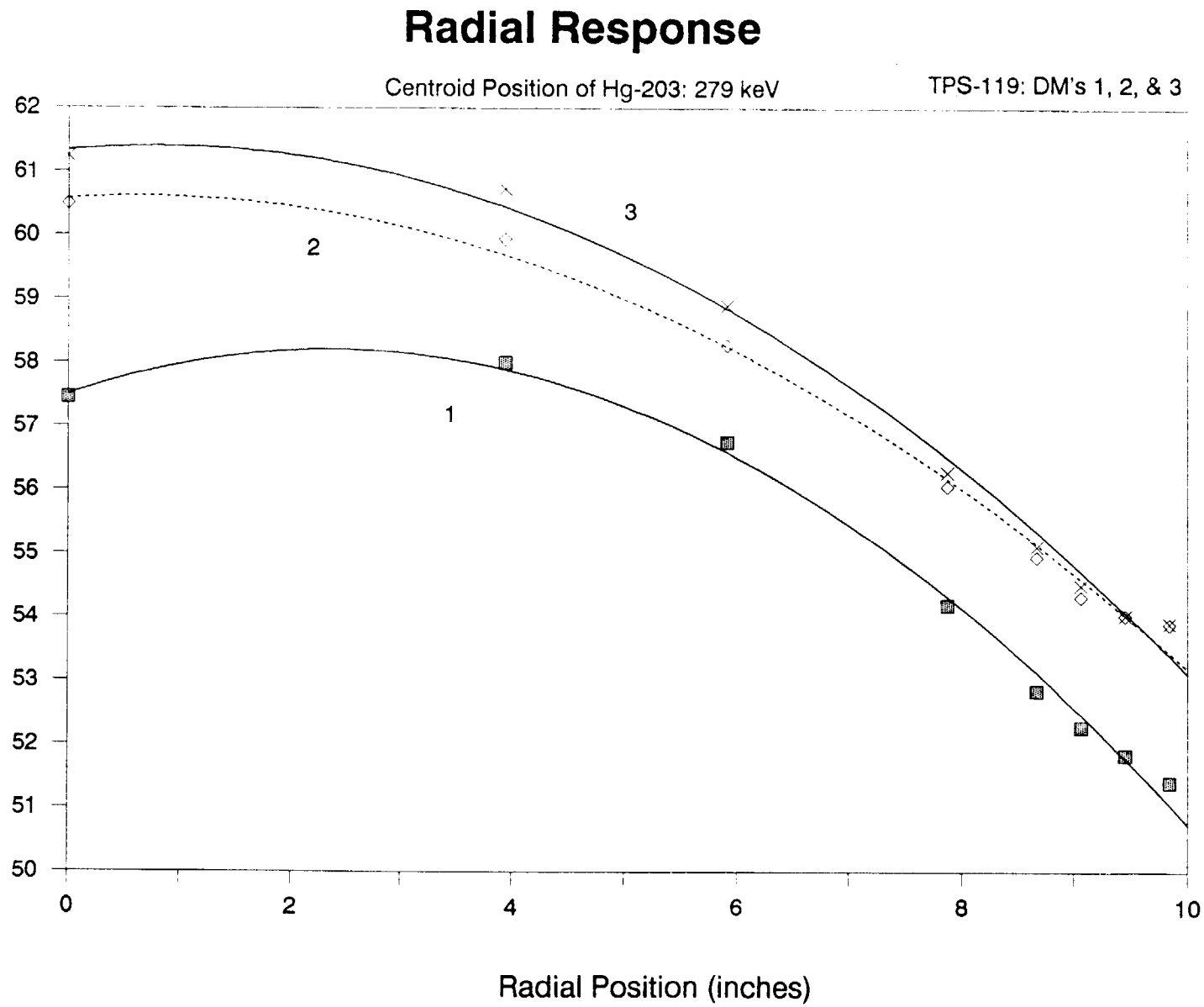
Radial Response
Centroid Position of Hg-203: 279 keV
TPS-119: DM's 1, 2, & 3
Centroid Channel
62
61
60
59
58
57
56
55
54
53
52
51
50
0
2
4
6
8
10
1
2
3
Radial Position (inches)

Figure 9

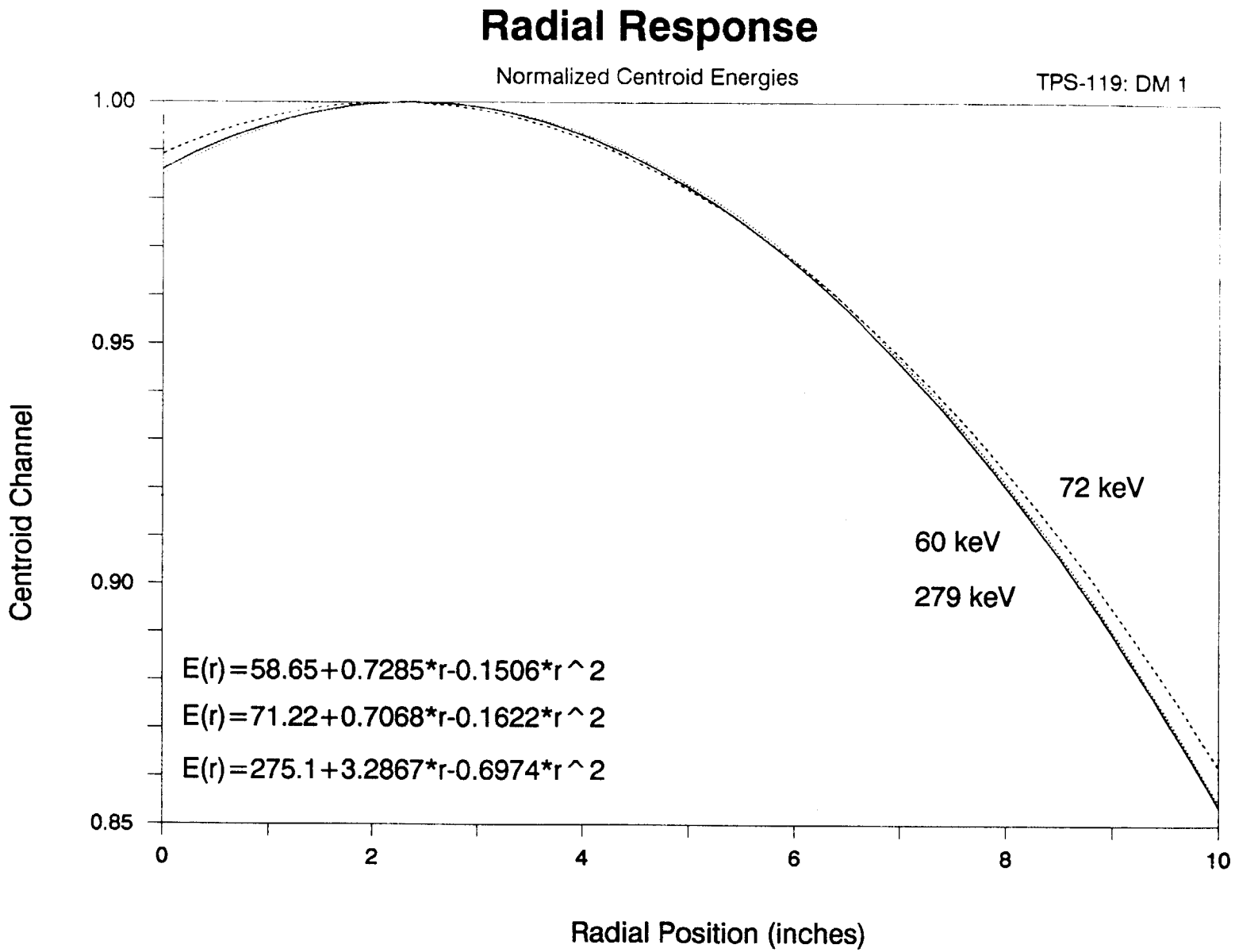
Radial Response
Normalized Centroid Energies
TPS-119: DM 1
1.00
0.95
0.90
0.85
Centroid Channel
72 keV
60 keV
279 keV
E(r)=58.65+0.7285*r-0.1506*r^2
E(r)=71.22+0.7068*r-0.1622*r^2
E(r)=275.1+3.2867*r-0.6974*r^2
0
2
4
6
8
10
Radial Position (inches)

Figure 10

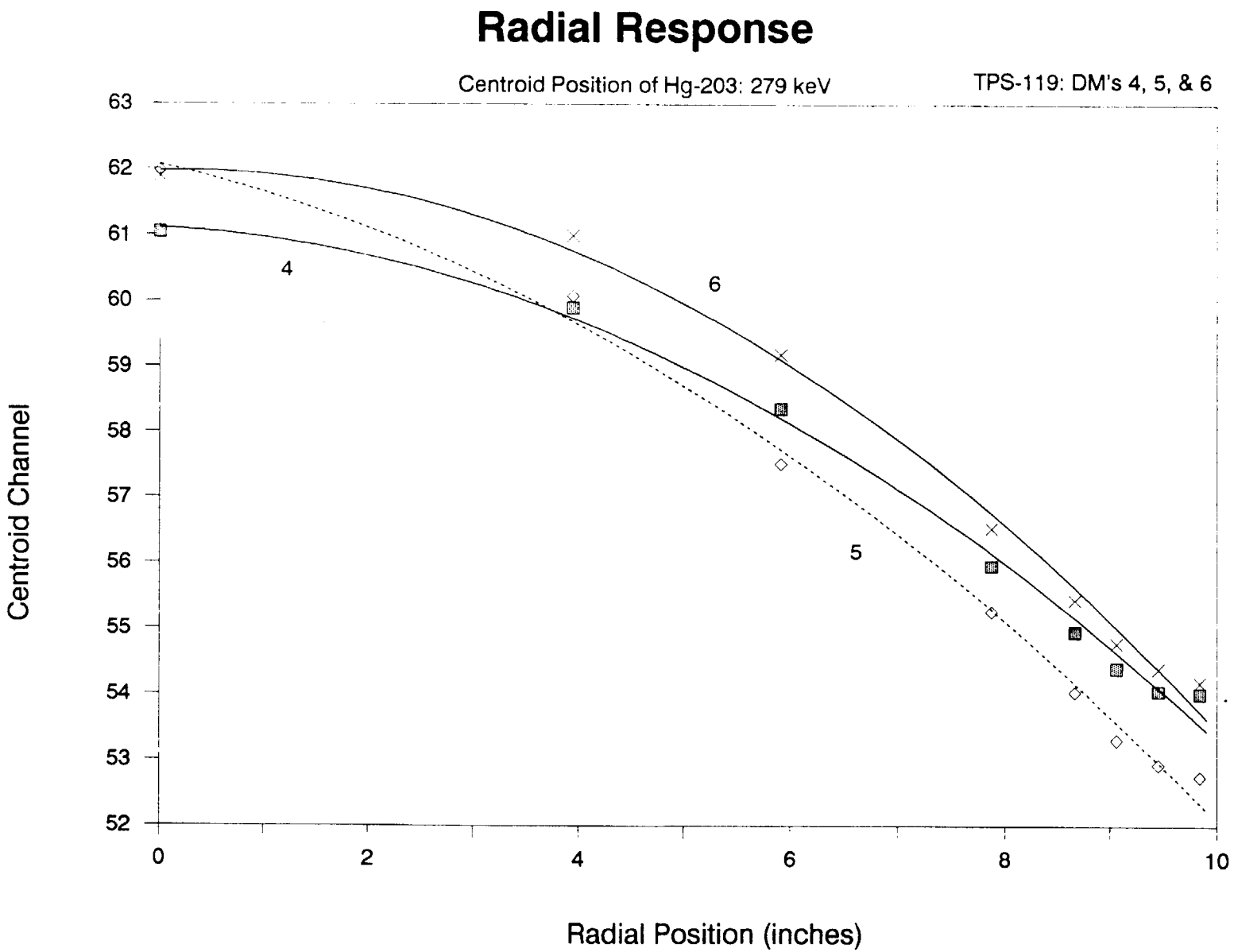
Radial Response
Centroid Position of Hg-203: 279 keV
TPS-119: DM's 4, 5, & 6
Centroid Channel
63
62
61
60
59
58
57
56
55
54
53
52
0
2
4
6
8
10
Radial Position (inches)
4
5
6

Figure 11

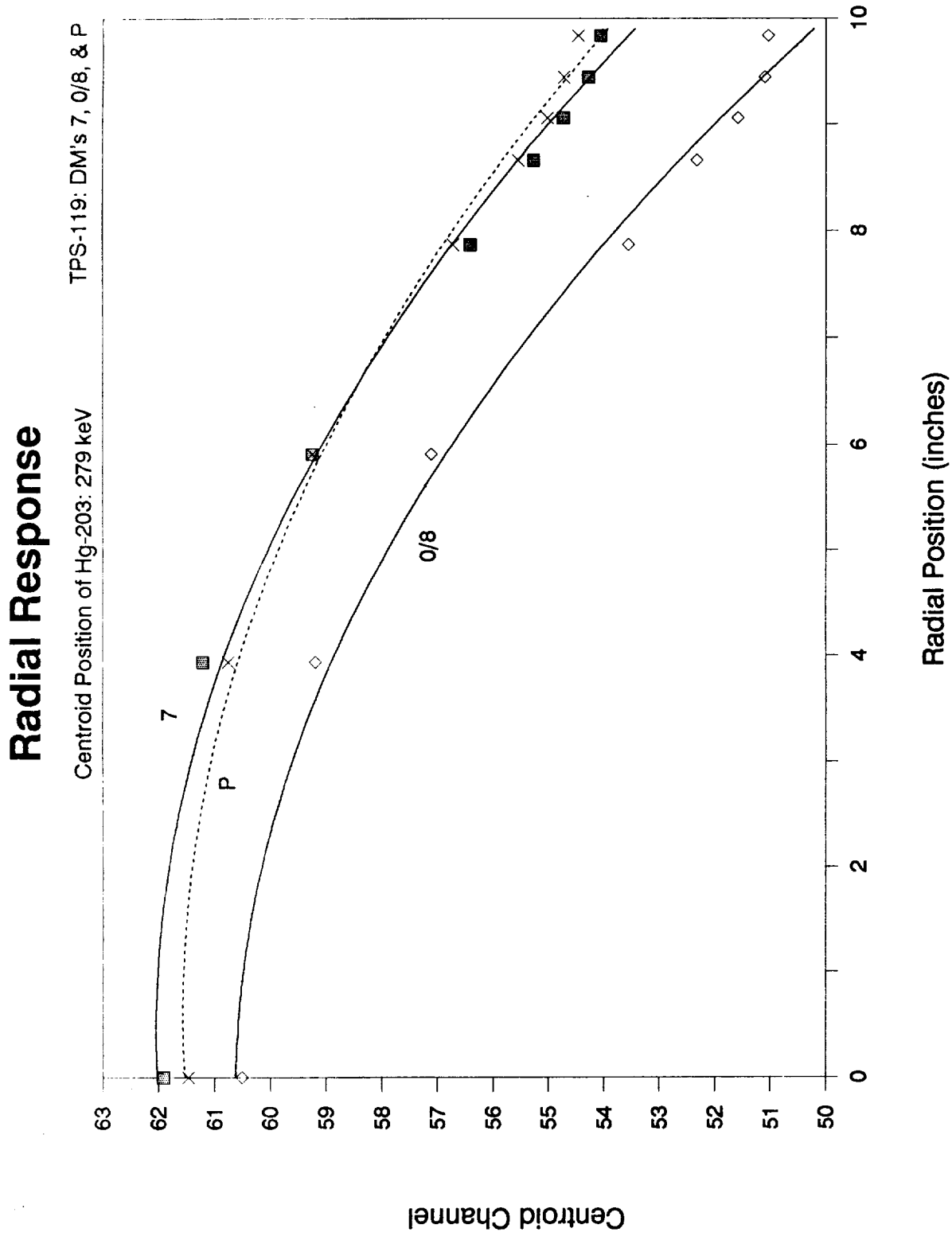
Radial Response
Centroid Position of Hg-203: 279 keV
TPS-119: DM's 7, 0/8, & P
7
P
0/8
Centroid Channel
Radial Position (inches)
63
62
61
60
59
58
57
56
55
54
53
52
51
50
0
2
4
6
8
10

Figure 12

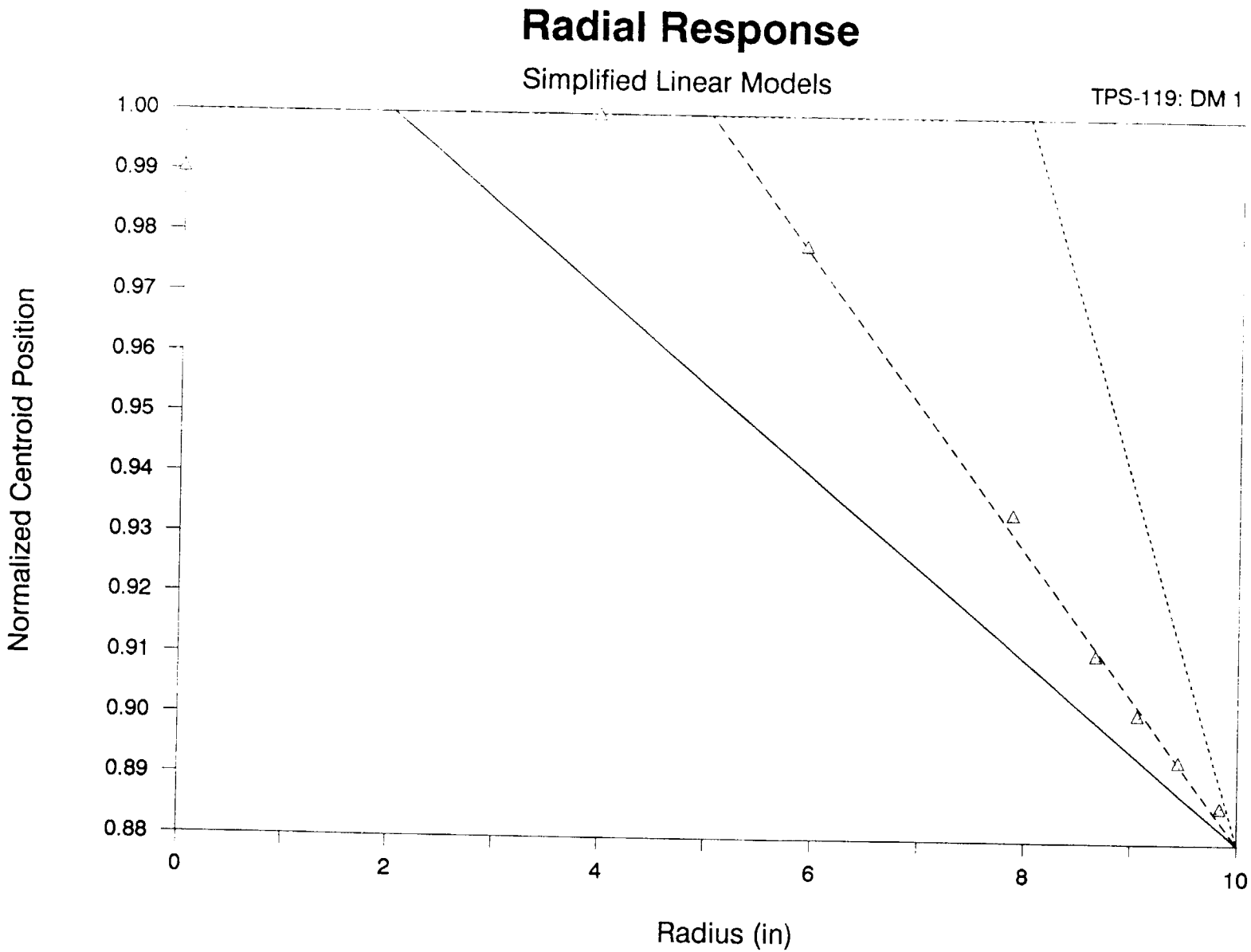
Radial Response
Simplified Linear Models
TPS-119: DM 1
Normalized Centroid Position
1.00
0.99
0.98
0.97
0.96
0.95
0.94
0.93
0.92
0.91
0.90
0.89
0.88
0
2
4
6
8
10
Radius (in)

Figure 13

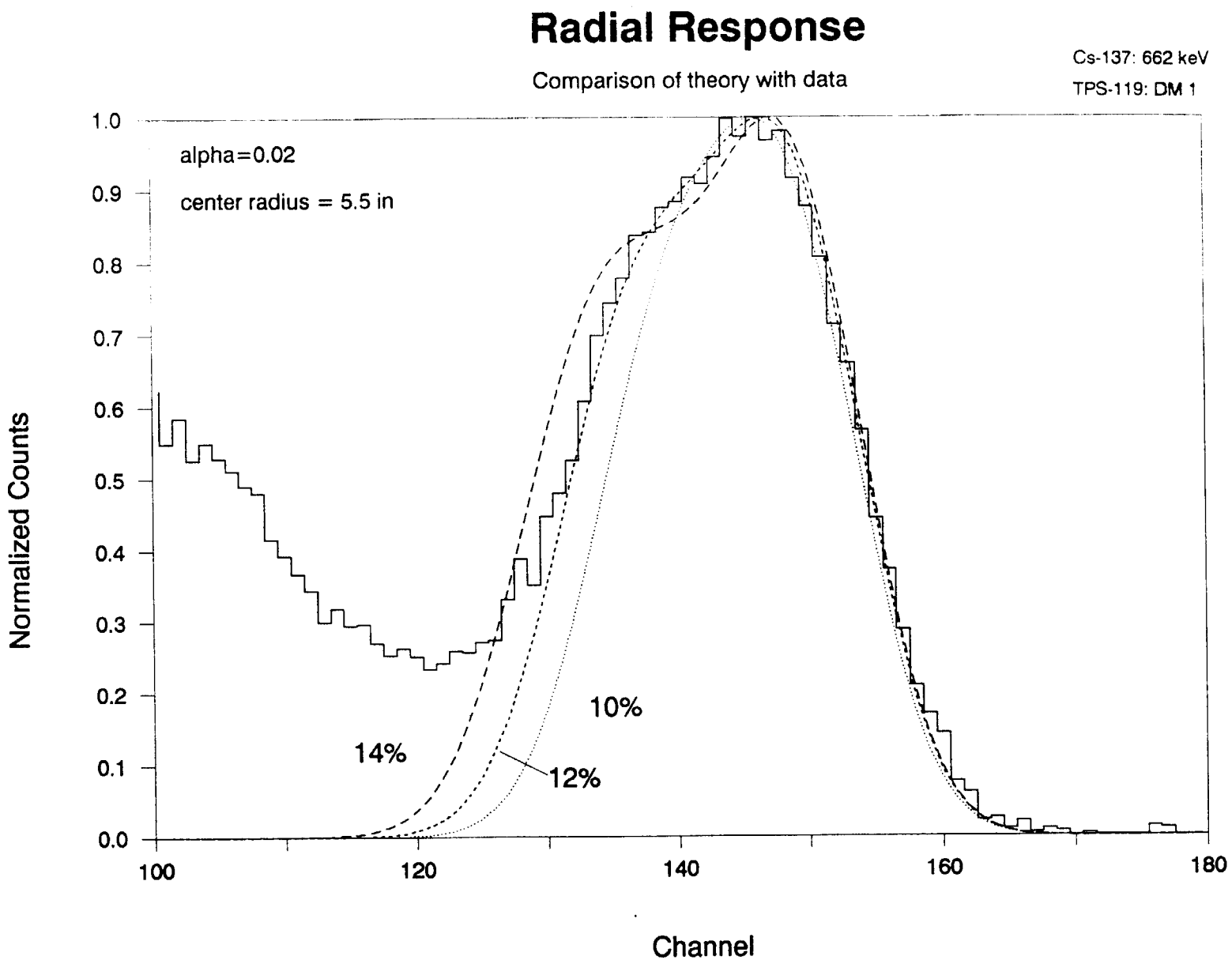
Radial Response
Comparison of theory with data
Cs-137: 662 keV
TPS-119: DM 1
alpha=0.02
center radius = 5.5 in
14%
12%
10%
Normalized Counts
Channel
1.0
0.9
0.8
0.7
0.6
0.5
0.4
0.3
0.2
0.1
0.0
100
120
140
160
180

Figure 14

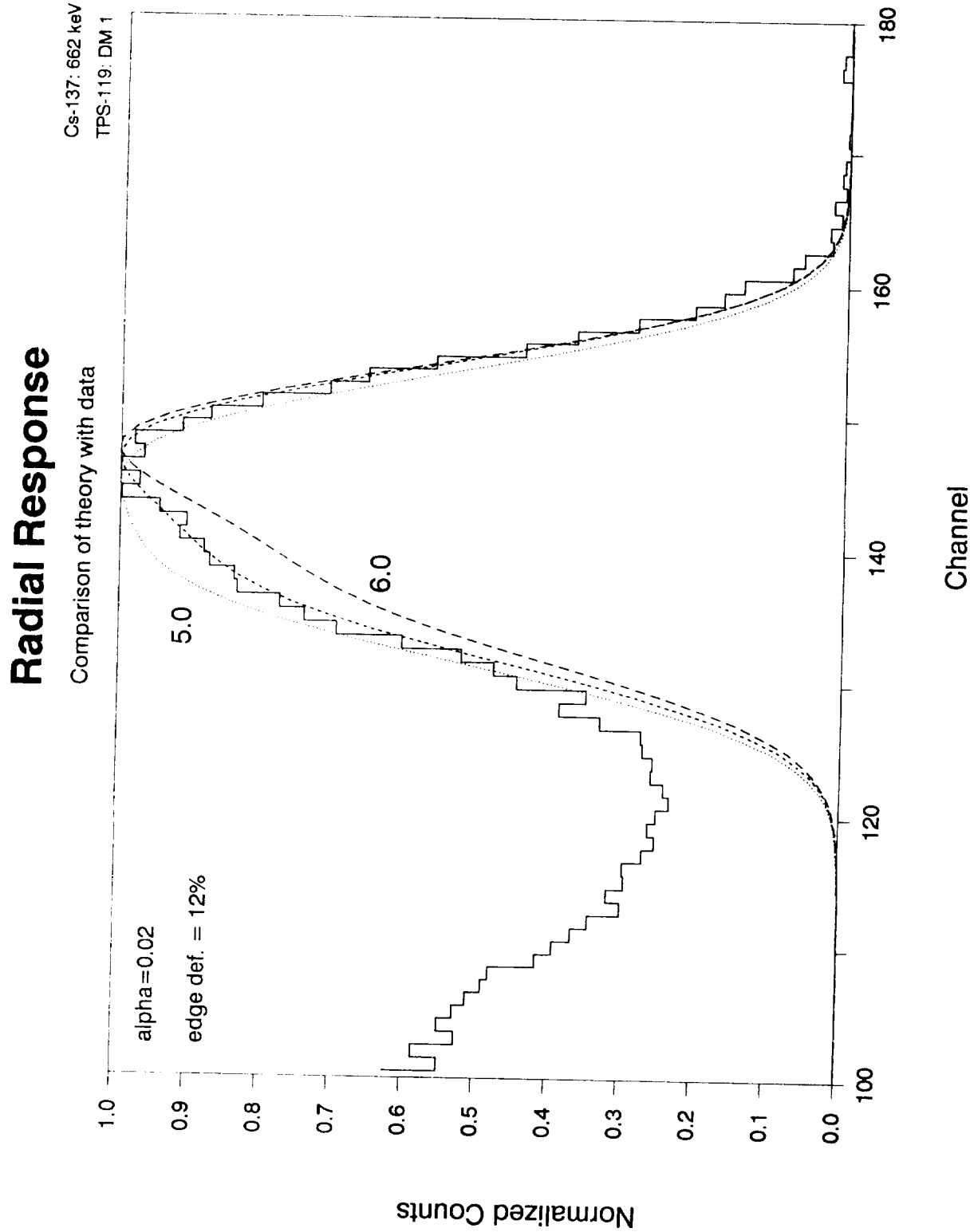
Radial Response
Comparison of theory with data
Cs-137: 662 keV
TPS-119: DM 1
alpha=0.02
edge def. = 12%
5.0
6.0
Normalized Counts
Channel
1.0
0.9
0.8
0.7
0.6
0.5
0.4
0.3
0.2
0.1
0.0
100
120
140
160
180

Figure 15

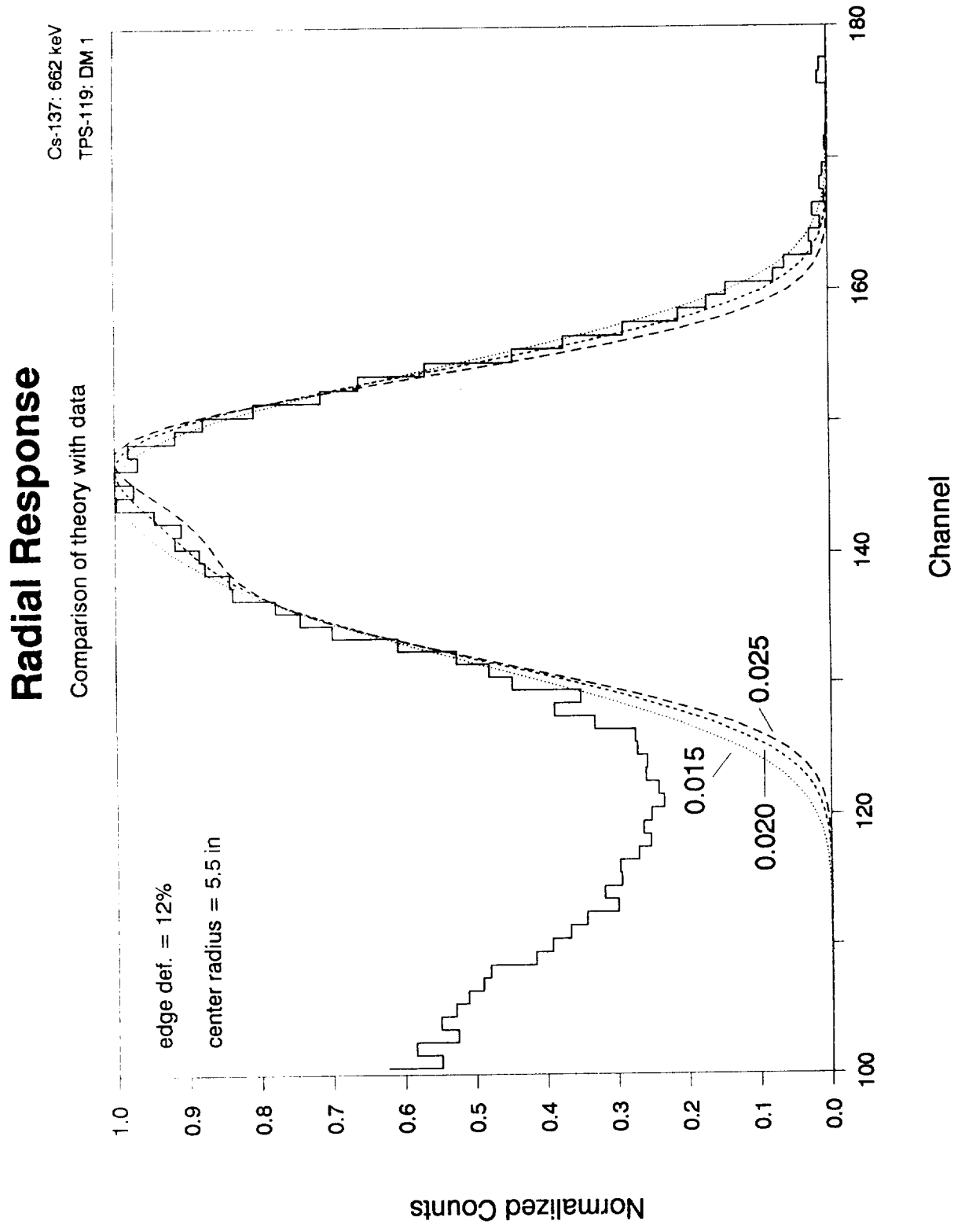
Radial Response
Comparison of theory with data
Cs-137: 662 keV
TPS-119: DM 1
edge def. = 12%
center radius = 5.5 in
0.015
0.020
0.025
Normalized Counts
Channel
1.0
0.9
0.8
0.7
0.6
0.5
0.4
0.3
0.2
0.1
0.0
100
120
140
160
180

Figure 16

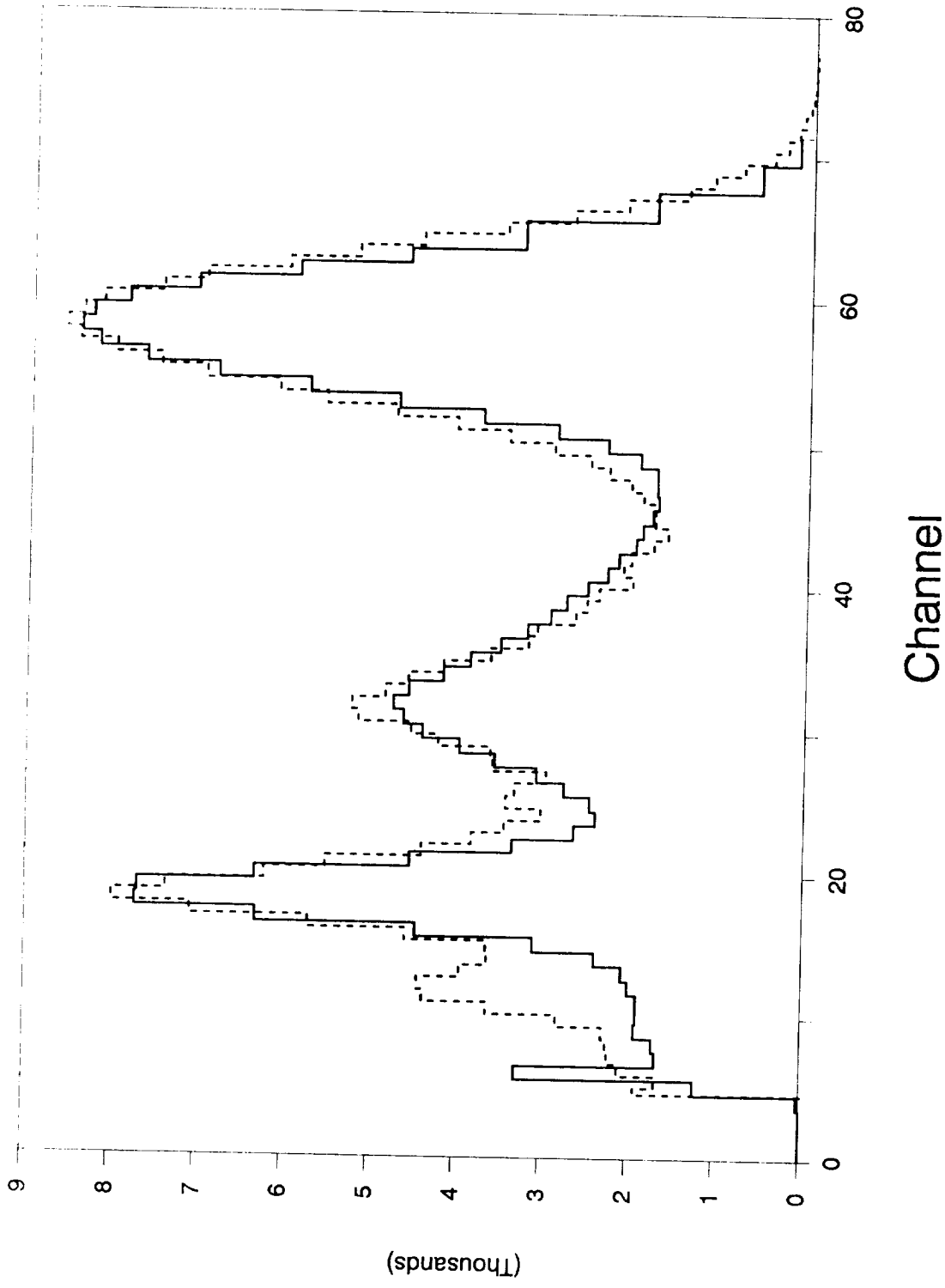

Figure 17